ISSN 0915-633X

NATIONAL INSTITUTE FOR FUSION SCIENCE

Identificaiton and Analysis of Vortical Structures

S. Kida and H. Miura

(Received - Nov. 4, 1997)

NIFS-520 Nov. 1997

RESEARCH REPORT
NIFS Series

NAGOYA, JAPAN

Identification and Analysis of Vortical Structures

S. KIDA and H. MIURA *

ABSTRACT. Various identification and visualization methods of vortical structure, especially of slender vortices, are critically reviewed with a special attention to their objectivity. The sectional-swirl-and-pressure-minimum scheme is presented as a new identification method and applied to homogeneous turbulence. Since the physical quantities associated with an individual vortex can be analyzed separately, this new scheme enables us to investigate quantitatively various physical characteristics related to vortices, such as the variations of the core shape, the circulation and the vorticity vector along a vortex and the temporal evolution of arbitrarily selected vortices.

For submission to Eur. J. Mech. B/Fluids
Keywords: Tubular vortex, vortex skeleton, swirl condition, turbulence

1 Introduction

Most flows of practical importance are rotational. Among various kinds of vortical motions, the existence of swirling slender vortices with relatively large vorticity is ubiquitous. The tornadoes in nature, the streamwise vortices in the turbulent shear flow with or without boundary, the Kelvin-Helmholtz vortex rolls and braids in the mixing layer and the tubular regions (so-called "worms") of high vorticity in isotropic turbulence are only some of typical examples ([Kim et al., 1971], [Siggia, 1981], [Bernal & Roshko, 1986], [Yamamoto & Hosokawa, 1990], [Lesieur and Métais, 1996] , [Kida & Tanaka 1994]). These structures are considered to be generated by various flow instabilities including the Kelvin-Helmholtz instability and intensified by vortex stretching ([Porter et. al., 1994], [Kida & Tanaka, 1994]).

The vortical motions make the fluid flow fully three dimensional and complicated in general, and play dynamically important roles in kinetic energy production and dissipation, mixing, diffusion and transport of mass, heat and momentum, enhancement of frictional drag in turbulent boundary layer, fluid instability, and so on. Understanding of the dynamics of the vortical structure, such as their generation, interaction and evolution mechanisms, is prerequisite for flow prediction and control.

*Theory and Computer Simulation Center, National Institute for Fusion Science, Oroshi 322-6, Toki, Gifu 509-52, JAPAN

Although such typical vortices mentioned above are relatively easily recognized, it is surprisingly difficult to define the general vortical structure objectively and unambiguously. There have been proposed so far a lot of methods of identification and visualization of swirling slender vortices with resort to various flow quantities such as streamlines, pathlines, vorticity, pressure, the Laplacian of pressure, the rate-of-strain tensor, etc. (see [Lugt, 1979], [Jeong & Hussain, 1995]). We must admit, however, that there is still no objective criterion found with which the vortical structure can be clearly educed and analyzed. Needless to say, it is helpful in the study of fluid dynamics to share a common idea or a consensus on the fundamental processes of fluid motions, e.g. on vortices and waves. In view of the universality of the existence of slender vortices the precise definition of them, if possible, is highly desirable.

In Sec. 2, various identification methods of vortical structures are discussed in the point of view of their objectivity. A new vortex eduction scheme is proposed in which the axis and the core of a vortex are determined by tracing the pressure-minimum line under the swirl condition. The advantage of vortex skeleton representation is presented. Then, this scheme is applied to homogeneous turbulence in Sec. 3. Section 4 is devoted to summary and further discussions.

2 Visualization of vortices

We survey here various methods of visualization of vortical structures with a special attention to the slender swirling vortices.

2.1. Velocity and vorticity representations

A precise definition of the vortical structure, if any, may be helpful not only for the description of fluid motions but also for the discussions on the vortex dynamics. The difficulty of the objective definition, however, has long been recognized among fluid dynamicists (see [Lugt, 1979]). For example, the streamlines or the pathlines are seen as spiral curves around a vortex by an observer who moves with that vortex. But we do not know a priori where the vortex in question is. This leads to a serious problem because the pattern of streamlines can be different among inertial systems with different velocity. Moreover, even if proper streamlines were obtained, it would not be easy to define the vortical domains from their three-dimensional pattern. In a special case that the direction of vortices is known a priori, however, the streamlines may be useful for identification at least approximately. In fact, the position and the core size of streamwise vortices in a wall turbulence were detected by analyzing the pattern of the streamlines projected on cross-stream planes [Bernard et al. 1993]. Since, however, the streamwise vortices are inclined quite a bit from the streamwise direction both to the wall-normal and the spanwise directions [see Jeong et. al. 1997], this method may suffer from ambiguity.

The vorticity, which is equal to a half of angular velocity of the rotation of fluid elements, is one of the most natural candidates for characterization of the vortical motions. A bundle

of vorticity lines were used for visualization of the vortical structure of tubular vortices in isotropic turbulence [She et al., 1991]. A hairpin vortex in wall turbulence was depicted in terms of vorticity lines [Moin & Kim 1982]. In spite of these suggestive studies, however, we must be careful in the vorticity-line representation. The vorticity lines are generally chaotic in fully-three-dimensional flows and the topology is structurally unstable. That is, the spatial structure of a vorticity line can change drastically by only a slight shift of it. Furthermore, the strength of vorticity is not represented by vorticity lines.

Instead of lines, the isosurfaces of vorticity magnitude have been used frequently to visualize the vorticity-concentrated regions in various turbulence partly because of its easy use. In fact, it was by this representation that tubular vortices in isotropic turbulence have called people's attention (see [Siggia, 1981], [Yamamoto & Hosokawa, 1988]). The formation of tubular vortices from flat vortical structures through the Kelvin-Helmholtz instability was observed in decaying isotropic turbulence [Porter et al., 1994]. The use of vorticity magnitude as representation of swirling tubular vortices, however, is problematic in at least the following two respects. First, soley the vorticity cannot distinguish the swirling motions from shearing. Recall that the Couette flow is rotational but all the streamlines are parallel. In fact the swirling tubular vortices and the shearing flat vortices are characterized by the use of relative magnitude of vorticity to the rate-of-strain [Tanaka & Kida, 1993]. Secondly, the geometrical structure of isosurface varies depending on the threshold, i.e. the value of the vorticity magnitude. Lower thresholds may provide flatter structures. Hence, this representation must be said to be subjective if the choice of the threshold is arbitrary.

A more elaborate characterization of the structure of the velocity field is given by the use of the velocity gradient (or the rate-of-deformation) tensor

$$W_{ij} = \frac{\partial u_i}{\partial x_j}. \tag{1}$$

A classification of the flow topology is made in terms of three invariants of $\underline{\boldsymbol{W}}$ as follows ([Dallmann, 1983], [Chong et al., 1990]).

Consider a topological structure of velocity field around an arbitrary point in a coordinate system moving with it. In the vicinity of this point the velocity field is approximated by

$$u_i = W_{ij} x_j, \tag{2}$$

the repeated suffices being summed up over 1—3. The eigenvalues λ of $\underline{\boldsymbol{W}}$ are calculated, for an incompressible flow, from

$$\lambda^3 + Q\lambda + R = 0, \tag{3}$$

where

$$Q = -\tfrac{1}{2} W_{ij} W_{ji} = -\tfrac{1}{2} \left(S_{ij} S_{ji} + \Omega_{ij} \Omega_{ji} \right) = -\tfrac{1}{2} \left(S_{ij} S_{ij} - \tfrac{1}{2} \omega_k \omega_k \right) = \tfrac{1}{2} \nabla^2 p \tag{4}$$

and

$$R = -\frac{1}{3}W_{ij}W_{jk}W_{ki} = \frac{1}{3}\left(S_{ij}S_{jk}S_{ki} + 3\Omega_{ij}\Omega_{jk}S_{ki}\right) \tag{5}$$

are the second and the third invariants of $\underline{\boldsymbol{W}}$, respectively, and $S_{ij} = \frac{1}{2}(W_{ij} + W_{ji})$ and $\Omega_{ij} = \frac{1}{2}(W_{ij} - W_{ji}) = -\frac{1}{2}\epsilon_{ijk}\omega_k$, ($\omega_i$ being the vorticity and ϵ_{ijk} the Eddington alternating tensor) are the symmetric and the anti-symmetric parts of the velocity gradient tensor, respectively. The last equality in (4) is derived by taking a divergence of the Navier-Stokes equation for an incompressible fluid of unit density.

Equation (3) can have either only real roots, or the one real root and a conjugate pair of complex roots according to whether the discriminant

$$\Delta \equiv \left(\frac{1}{3}Q\right)^3 + \left(\frac{1}{2}R\right)^2 \tag{6}$$

is non-positive or not. If the eigenvalue is complex at some point, the streamlines around this point form in general spiral curves on a plane spanned by the real and the imaginary parts of the eigenvector associated with this complex eigenvalue. The regions in which the eigenvalues of the velocity gradient tensor are complex may be regarded as "vortex" ([Dallmann, 1983], [Chong et al., 1990]). This definition ($\Delta > 0$) of vortical regions will be applied to homogeneous turbulence in the next section. Note that the discriminant is non-positive ($\Delta \leq 0$) for an irrotational flow ($\underline{\boldsymbol{\Omega}} = \underline{\boldsymbol{o}}$) (the equality holds for any two of the eigenvalues are equal), and that if $Q > 0$, then $\Delta > 0$.

2.2 Pressure representation

Around the center of a swirling vortex the pressure is likely to be reduced to counterbalance the centrifugal force. This fact suggests a possible use of low-pressure regions for eduction of vortices. In fact, the pressure has been used by many researchers for characterization of flow structures, such as a classification of the flow structure [Wray & Hunt, 1990] and a better identification of vortical regions in a two-dimensional flow [Iwayama & Okamoto, 1996]. The superiority of the vortex visualization by pressure over the vorticity magnitude in mixing layer turbulence is noticed by Métais & Lesieur (1992). The low-pressure regions are easily visualized by bubbles in laboratory experiments. The existence of low-pressure slender vortices in rotating turbulence was reported by Douady et al. (1991).

One important thing to be noticed in the pressure representation is that the lowness of the pressure inside a swirling vortex is relative to the surroundings and that the absolute value of the pressure depends on the surrounding pressure distribution. This may bring a serious difficulty in visualizing many vortices at a single level of pressure. The visualization of vortices by pressure therefore may not be appropriate for such a system in that many vortices coexist, though it can work as a good indicator for detection of a few strong vortices. Since the choice of the threshold is arbitrary, this method is not objective.

Another fundamental question is that the low pressure does not necessarily imply the existence of swirling motion, and vice versa. There is an unsteady flow in which the pressure is lower even if there is no swirling motion. On the other hand, the pressure does not take a minimum across a stationary Kármán swirling vortex [Jeong & Hussain 1995]. Our new swirl condition will be discussed in §2.4.

As mentioned above, the pressure level inside of vortices depends on the surrounding flow field and it is not appropriate to visualize many vortices simultaneously. One of the quantities which are free from this drawback but still capable of representing the lower pressure is the Laplacian of pressure $\nabla^2 p$. As shown in (4), this expresses the difference in magnitude between the anti-symmetric and the symmetric parts of the velocity gradient tensor, or the relative magnitude of the vorticity and the strain rate. It was observed in homogeneous shear turbulence that tubular vortices and flat vortical regions appear in the vorticity- and the strain-dominant regions, respectively [Tanaka & Kida, 1993]. Since, however, the threshold is set arbitrarily, this method cannot escape from subjectivity.

The above argument on the low pressure inside a vortex is applied across the vortex but not along it. That is, the pressure does not necessarily take a minimum along a vortex. This condition is expressed mathematically as that at least two eigen-values of the pressure hessian $(\partial^2/\partial x_i \partial x_j)p$ are positive. A consideration of extracting the effects of pressure on swirling motion has recently been made by Jeong & Hussain (1995). By removing the effects of unsteadiness and viscosity, which have no direct connection with swirling motions, from the Navier-Stokes equation, they took $-(S_{ik}S_{kj} + \Omega_{ik}\Omega_{kj})$ in place of the pressure hessian and defined a vortex core as such regions in that two eigenvalues of $-(S_{ik}S_{kj} + \Omega_{ik}\Omega_{kj})$ are positive. Note that a set of the eigenvalues of $-(S_{ik}S_{kj} + \Omega_{ik}\Omega_{kj})$ does not, in general, coincide with that of the pressure hessian though the sum of the three eigenvalues does. Therefore the pressure does not always take a minimum across the regions extracted by this method. They applied this definition (called λ_2-definition by them) to several typical flows with clear vortical structures and showed that it is superior to other methods in many respects. This is an objective definition of vortical structure. If this method is applied to homogeneous turbulence, however, the isosurfaces cover too much amount of the space to visualize the vortex structure neatly [Miura & Kida, 1997]. Note also that contrary to the λ_2 definition, a non-zero threshold for λ_2 is employed in the eduction of the longitudinal vortices in wall-turbulence [Jeong et al., 1997].

2.3. Vortex skeleton

In all the visualization methods of vortical regions discussed in the preceding subsections a finite volume of vortical regions are dealt with. The size, shape and position of vortical regions not only change in time but also vary from vortex to vortex. Enormous amount of memory and computation time are necessary to represent the whole structure and their temporal evolution

of such vortex regions.

On the other hand, it is now commonly believed that tubular vortices are dominant in most turbulent flows. The core radius, which is several times of the Kolmogorov length (see §3), decreases with Reynolds number. If a vortex is sufficiently thin, we may represent it by the central axis with disregarding the core. This is called the vortex skeleton. (The representation of core will be considered in §2.4.)

The skeleton representation has the following merits. First, the amount of data size necessary to represent a vortex and the computation load can be drastically reduced. This makes it possible to describe, for example, the temporal evolution of a vortex. Secondly, each vortex can be marked independently. This enables us to visualize only a few of arbitrarily chosen vortices. (It is impossible for isosurface representation of a scalar variable to distinguish the individual vortical structure.) Then, we can investigate the temporal evolution of chosen vortices from their birth to the death, and mutual interactions, collision, breakdown, instability, etc. Thirdly, by constructing the core around the axis (e.g. by the use of the swirl condition described in §2.4), we may analyze the temporal evolution of the core deformation. A quantitative analysis of various physical quantities related to vortices is also possible, such as the contributions from vortices to the enstrophy and energy-dissipation rate.

The vortex skeleton is constructed for example by tracing the lines of sectional pressure minimum introduced in the preceding subsection. The pressure minimum was searched in planes normal either to the vorticity [Banks & Singer 1995] or to the third eigenvector, which is the one associated with the smallest eigenvalue, of the pressure hessian [Miura & Kida 1997]. Existence of the swirling motions around these skeletons has been demonstrated in Fig. 2 in Miura & Kida (1997). These two methods are expected to give comparable results for strong slender vortices for which the above two planes are more or less parallel (see Fig. 5(a)). The vortex core is determined by setting an appropriate threshold of the pressure in the former and by the swirl condition (§2.4) in the latter. Note that the latter scheme is objective, but the former is not. The vortex identified by these schemes may conveniently be called the low-pressure vortex. An application of the latter scheme to homogeneous turbulence will be presented in §3. Other methods of skeleton construction have been proposed by Villasenor & Vincent (1992) and by Jiménez et al. (1993), in which the regions of strong vorticity are searched for.

2.4 Swirl condition

As mentioned in §2.2, a swirling motion is not always associated with a sectional pressure minimum. In order to educe only swirling vortex we impose it a swirl condition.

Let us take an arbitrary point in a flow and consider the topological structure of the velocity field in a plane passing it. Let us choose a Cartesian coordinate system (x_1, x_2, x_3) which moves with the fluid velocity at the above point and whose x_1 and x_2 axes lie on the above plane. In

the vicinity of this point, the velocity projected on the (x_1, x_2) plane is written as

$$u_1 = W_{11}x_1 + W_{12}x_2, \tag{7}$$

$$u_2 = W_{21}x_1 + W_{22}x_2 \tag{8}$$

(see (2)). The topological structure of the streamlines is characterized by the sign of the discriminant of the (2,2)-matrix $\{W_{ij}\}$ $(i, j = 1, 2)$,

$$D = \tfrac{1}{4}(W_{11} - W_{22})^2 + W_{12}W_{21}. \tag{9}$$

The streamlines spiral around the origin or not according to whether D is negative or not. (If an axi-symmetric source or sink flow centered at the origin ($u_i = \frac{1}{2}(W_{11} + W_{22})x_i$, $i = 1, 2$) is subtracted, the streamlines of the remaining solenoidal flow field form ellipses or hyperbolas according as $D < 0$ or $D > 0$.) The elliptical regions may be regarded as vortex ([Weiss, 1991], [McWilliams, 1984], [Brachet et al., 1988]). Note that $D = -Q = -\frac{1}{2}\nabla^2 p$ in the two-dimensional incompressible flow ($W_{11} + W_{22} = 0$), and therefore the definition ($Q > 0$) of vortical region is equivalent to the above definition.

In order to check the rationality of the above definitions of vortical structures we apply it to a Burgers vortex tube, the velocity field of which is written in a cylindrical polar coordinate system (r, θ, z) as

$$u_r = -\tfrac{1}{2}\alpha r, \tag{10}$$

$$u_\theta = \frac{\Gamma}{2\pi r}\left\{1 - \exp\left[-\frac{\alpha}{4\nu}r^2\right]\right\}, \tag{11}$$

$$u_z = \alpha z, \tag{12}$$

where α (> 0) and Γ are constants.

The vorticity is pointed to the z-direction and is written as

$$\omega_z = \frac{\alpha\Gamma}{4\pi\nu}\exp\left[-\frac{\alpha}{4\nu}r^2\right]. \tag{13}$$

The 1/e (≈ 0.37) radius of the vorticity core is $2\sqrt{\nu/\alpha}$. The pressure is given by

$$\frac{p}{\rho} = -\tfrac{1}{2}\alpha^2 z^2 - \tfrac{1}{8}\alpha^2 r^2 - \left(\frac{\Gamma}{2\pi}\right)^2 \int_r^\infty \frac{1}{r_1^3}\left\{1 - \exp\left[-\frac{\alpha}{4\nu}r_1^2\right]\right\}^2 \mathrm{d}r_1 + const. \tag{14}$$

The azimuthal velocity u_θ has a peak at $r_* \approx 2.24\sqrt{\nu/\alpha}$, at which the vorticity is smaller than that at the center by a factor of 0.18. The circulation and the enstrophy included in a circular cylinder of radius r_* are about 82% of the total. The discriminant D takes negative values at $r < r_*$ so that the present definition of vortex specifies the core region of a Burgers vortex tube unambiguously. On the contrary, the pressure depends on the strength α of the converging flow. The definition of vortical structure by the use of pressure, such as $\partial^2 p/\partial r^2$, therefore cannot be universal.

Next we extend the above swirl condition to a plane of arbitrary orientation. To do it we introduce a rotation of the coordinate system in which the original Cartesian coordinate system (x_1, x_2, x_3) is rotated around the x_3-axis by angle ϕ $(0 \leq \phi < 2\pi)$ and around a new x_2-axis by angle θ $(0 \leq \theta \leq \pi)$. The velocity field (u_1^*, u_2^*, u_3^*) in the new coordinate system (x_1^*, x_2^*, x_2^*) is then expressed as

$$u_i^* = M_{ia} W_{ab} \widetilde{M}_{bj} x_j^* \ (\equiv W_{ij}^* x_j^*, \text{say}), \tag{15}$$

where

$$\underline{\boldsymbol{M}} = \begin{pmatrix} \cos\theta\cos\phi & \cos\theta\sin\phi & -\sin\theta \\ -\sin\phi & \cos\phi & 0 \\ \sin\theta\cos\phi & \sin\theta\sin\phi & \cos\theta \end{pmatrix} \tag{16}$$

is a rotation matrix and $\underline{\widetilde{\boldsymbol{M}}}$ is its inverse. The swirl condition in the (x_1^*, x_2^*) plane is written as

$$\begin{aligned} D(\theta,\phi) &= \tfrac{1}{4}(W_{11}^* - W_{22}^*)^2 + W_{12}^* W_{21}^* \\ &= \tfrac{1}{4}\Big[(\cos^2\theta\cos^2\phi - \sin^2\phi)W_{11} + (\cos^2\theta\sin^2\phi - \cos^2\phi)W_{22} + \sin^2\theta W_{33} \\ &\quad +(\cos^2\theta + 1)\sin\phi\cos\phi(W_{12} + W_{21}) - \sin\theta\cos\theta\sin\phi(W_{23} + W_{32}) \\ &\quad -\sin\theta\cos\theta\cos\phi(W_{31} + W_{13})\Big]^2 \\ &\quad +\Big[\cos\theta\cos\phi\sin\phi(W_{22} - W_{11}) + \tfrac{1}{2}\cos\theta(\cos^2\phi - \sin^2\phi)(W_{12} + W_{21}) \\ &\quad -\tfrac{1}{2}\sin\theta\cos\phi(W_{23} + W_{32}) + \tfrac{1}{2}\sin\theta\sin\phi(W_{31} + W_{13})\Big]^2 \\ &\quad -\tfrac{1}{4}\Big[\cos\theta(W_{12} - W_{21}) + \sin\theta\cos\phi(W_{23} - W_{32}) + \sin\theta\sin\phi(W_{31} - W_{13})\Big]^2. \end{aligned} \tag{17}$$

It is obvious that $D(\theta, \phi) \geq 0$ for an irrotational flow in which the anti-symmetric part of the velocity gradient tensor vanishes. Moreover, it is easily shown that there exists a direction (θ, ϕ) for which $D(\theta, \phi) = 0$ in any points of an irrotational flow. This means that at any point in rotational regions (where the vorticity is not zero) there is a plane on which the instantaneous streamlines relative to the velocity at this point are elliptical. In other words, if we define the vortical regions as those at which the minimum (over all the orientations) of D is negative, then it covers the whole space. Incidentally, the sectional swirl of streamlines in a plane does not necessarily mean the spiral form of the streamlines viewed from the direction normal to the plane.

The swirl condition $(D(\theta, \phi) < 0)$ is used to supplement the sectional-pressure-minimum scheme for the purpose of picking up swirling vortices. Here, the angles (θ, ϕ) are given by the direction of the third eigenvector of the pressure hessian. [1] The vortex core is defined as

[1] About 20% of the candidates of the skeletons are discarded by this condition in homogeneous turbulence discussed in §3.

the regions of $D(\theta, \phi) < 0$ surrounding the vortex axis. This definition (called the sectional-swirl-and-pressure-minimum scheme) of the axis and the core of vortices will be applied to homogeneous turbulence in the next section.

3 Vortical structures in homogeneous turbulence

In this section the low-pressure vortices in freely decaying homogeneous turbulence are visualized by making use of the sectional-swirl-and-pressure-minimum scheme described in the preceding section.

3.1. Isotropic Turbulence

The vortical structure in an isotropic turbulence is analyzed by the use of the data obtained by a direct numerical simulation of the Navier-Stokes equation in a periodic cube of side 2π. The initial velocity field is given in the spectrum representation with a prescribed energy spectrum $E(k) = (k/k_0)^4 \exp\left[-2(k/k_0)^2\right]$ ($k_0 = 4$) with randomized phases. The dealiased (by the shifted-grid technique) spectral method is used for the spatial integro-differential operations with resolution $N^3 = 128^3$. The temporal marching is performed by the fourth-order Runge-Kutta scheme with time step $\Delta t = 0.5$. The viscosity is set at $\nu = 5 \times 10^{-5}$.

The enstrophy increases at first, takes a maximum and then decreases in time. Here, we take a flow field at a time after the enstrophy maximum by which the smallest scales of motion are fully excited and the tubular vortices are well developed. The Taylor micro-scale length λ and the Kolmogorov length $l_K = \epsilon^{-\frac{1}{4}} \nu^{\frac{3}{4}}$ at this time are 0.31 and 0.028, respectively, which may be compared with the effective mesh-size of the simulation $\Delta x = 2\pi/128 = 0.049$. The micro-scale Reynolds number R_λ is 46.

In Figs. 1, we plot the isosurfaces of (a) the vorticity magnitude and (b) the Laplacian of pressure. The thresholds of these surfaces are chosen in such a way that they cover the 5% of the total volume. In the both figures tubular vortical structures are prominent. They look quite similar as a whole, but the layer structures are also conspicuous in the vorticity magnitude. It should be remembered here that the appearance of the vortical structures displayed by these traditional visualizations does change substantially depending upon the value of the arbitrarily chosen threshold. That is, they are not objective visualizations.

The central axes of swirling vortices constructed by the sectional-swirl-and-pressure-minimum scheme are drawn with a series of segments of length of order Δx in Fig. 2. There are 13302 vortices and the total length of them is 1660 ($= 33810\Delta x$). The mean length of the vortices is 0.12 ($= 2.5\Delta x$), the maximum is 4.1, and the majority (50%) is concentrated in range between 0.1 and 0.5. Note, however, that since each vortex is easily torn apart by the mutual interactions, it is not so meaningful to speak about their mean length. As discussed in Miura & Kida (1997), all the skeltons of low-pressure vortices are not included in the isosurfaces of the vorticity magnitude nor the Laplacian of pressure.

In order to see the characteristic features of the vortices in more detail we plot in Fig. 3(a) the variations of D (solid line), $\frac{1}{2}|\omega|^2$ (thick broken line), p (dotted line) and $\nabla^2 p$ (thin broken line) along the axis of an arbitrarily chosen vortex (the light-blue one in Fig. 7). The abscissa is the arc-length s (measured from the right-end of the above vortex in Fig. 7) scaled by mesh-size Δx. The axial length of this vortex is $50\Delta x$. It is remarkable that there is a strong correlation among the variations of three physical quantities, namely, $\frac{1}{2}|\omega|^2$, $\nabla^2 p$ and $-D$ change in the same sense, and also a weak correlation with $-p$. A similar behavior is observed in other vortices as well. This favors that either high $|\omega|^2$, high $\nabla^2 p$, low p or low D has often been used for the visualization of vortices.

The cross-sections of the core (defined as the region where $D < 0$) of this vortex, are depicted over the whole vortex in Fig. 3(b). The ordinate is normalized by the Kolmogorov length. It is seen that the shape of the cross-section varies substantially from place to place, which is commonly observed in other vortices as well. The variation of the cross-section in range $25 < s/\Delta x < 35$ (around the lowest D) is focused in Fig. 3(c). The shape is roundish and stable in this range.

The radius from the center to the periphery of the core varies in general with the direction (see Figs. 3(b) and (c)). The mean (thick line) and the standard deviation (broken line) along the vortex axis are shown in Fig. 4(a). The mean value is more or less stable especially where the core is round (see Fig. 3(c)).

It is not easy to estimate the mean core radius of vortices because both the shape and the area change a lot from vortex to vortex. But since the core of long vortices is relatively round, we may define reasonably well the mean radius of relatively long vortices. The mean radius averaged over the whole vortices is $3.2l_K$, while it is $3.8l_K$ for vortices whose length is larger than the mean. The mean value increases with the threshold of the length and approaches around $4.5l_K$. Here, the average has been taken over relatively round cores whose radius does not exceed $\pm 30\%$ of the mean in all directions. Comparable values were obtained before by Jiménez et al. (1993) and Tanahashi et al. (1997). In the latter the azimuthal velocity is shown to be well approximated by that of the Burgers vortex (11).

The distribution of the circulation Γ along the vortex axis is shown in Fig. 4(b). Here, the circulation is calculated by a direct numerical integration of the velocity around the periphery of the core. It varies gradually except for a rather rapid change around $s/\Delta x = 20$. It takes about 0.011 and 0.005 in the right and left parts, respectively. The vortex Reynolds number $R_\Gamma = \Gamma/\nu$ is 220 and 100 in the respective parts. These values may be compared with $R_\Gamma \approx 126$ at $R_\lambda \approx 36$ and $R_\Gamma \approx 135$ at $R_\lambda \approx 63$ which are reported by Jiménez et al. (1993). The reduction of the circulation in the left may be attributed to a tear-off of the vortex core by a nearest vortex tube (see Fig. 6(b) below).

The variations of the directions of the third eigenvector of the pressure hessian (solid line)

and the vorticity (broken line) along the above vortex are shown in Fig. 5(a), in which the angles of these vectors from the skeleton are plotted. The angles between the two vectors as well as between consecutive segments are shown in Figs. 5(b) and (c), respectively. It is seen that both of the angles shown in Fig. 5(a) are relatively small (about 10^o or less) over the whole range except at the very right end. This suggests that the two skeleton construction schemes by the use of either vorticity or the pressure hessian (see §2.3) give comparable results though the latter seems slightly better. This angle in the latter should tend to zero in the limit of infinite resolution ($\Delta x \to 0$). The large values at the end indicate that the vortex is kinked strongly there (see Fig. 5(c)).

The vortical regions surrounding vortex skeletons are educed by the sectional-swirl-and-pressure-minimum scheme described at the end of the preceding subsection. They occupy 33% of the total volume which is so large that the core structure can hardly be seen by plotting the core boundary (figures omitted). The enstrophy included in these vortical regions is 48% of the total. Incidentally, the vortical regions defined by $\Delta > 0$ and $\nabla^2 p > 0$ occupy 65% and 43% of the total volume, respectively. These are again too much for the isosurfaces to visualize the structure well. In our method, however, a seeable visualization of vortices is possible because any vortex skeletons can be chosen and marked arbitrarily. In Fig. 6(a), we select 13 vortices whose core regions are drawn with colored surfaces. The vortex presented in Figs. 3-5 is the light-blue one. Figure 6(b) is a close-up of this vortex. It is clearly seen that the core is gouged out by a nearest vortex (green).

3.2. Homogeneous Shear Turbulence

The data of homogeneous shear turbulence which is analyzed here is the one that was simulated by Kida & Tanaka (1992, 1994). The simulation was started with a random velocity field superimposed to a uniform mean shear flow $\overline{u}_1 = Sx_2$, where S $(= 10)$ is the shear rate. The subscripts 1, 2 and 3 denote the streamwise, the vertical and the spanwise directions, respectively. The fluctuating field is periodic with periods 4π, 2π and 2π in the x_1-, the x_2- and the x_3-directions, respectively. The spatial integro-differential operations were made by the spectral method with resolution of $N^3 = 128^3$. Then the effective mesh-sizes are $\Delta x_1 = 0.098$ and $\Delta x_2 = \Delta x_3 = 0.049$. The Runge-Kutta-Gill scheme with time step $\Delta t = 0.002$ was employed for temporal marching.

In Figs. 7, we plot the isosurfaces of (a) the vorticity magnitude and the Laplacian of pressure and (c) their union at $St = 8$ by which turbulence has been well developed. Here, a quarter of the fundamental periodic box ($0 \le x_1 \le 4\pi$, $0 \le x_2, x_3 \le \pi$) are shown. The levels of the isosurfaces are chosen in such a way that they include the 5% of the total volume. The oblique vortical structure inclined vertically from the streamwise direction is common in the both fields. However, the shape of the structure is much different from each other. It is flat in the vorticity magnitude, whereas tubulous in the Laplacian of pressure. Most

tubular structures of vorticity magnitude are included in the isosurfaces of $\nabla^2 p$, while the flat structures are outside. (see Tanaka & Kida, 1993). Incidentally, the root-mean-square of the vorticity magnitude is $\sqrt{\langle|\omega|^2\rangle} = 11$ which is comparable with the mean shear vorticity $S = 10$, and the three components of vorticity are of comparable orders, $\sqrt{\langle\omega_1^2\rangle} = 11$, $\sqrt{\langle\omega_2^2\rangle} = 10$ and $\sqrt{\langle\omega_3^2\rangle} = 15$.

The vortex skeletons constructed by the sectional-swirl-and-pressure-minimum scheme are drawn in Fig. 8. There are 2775 vortices and the total length is 311 ($= 6328\Delta x_2$). The mean length of the vortices is then 0.11 ($= 2.3\Delta x_2$). The Kolmogorov length at this time is $l_K = 0.023$. All the skeltons are again not included in the isosurfaces of vorticity magnitude nor the Laplacian of pressure (figures omitted).

The variations of D, $\frac{1}{2}|\omega|^2$, p and $\nabla^2 p$ along the axis of a vortex (the lower-right one in Fig. 10) are plotted in Fig. 9(a). The meaning of the lines is the same as Figs. 3(a). The arc-length is measured from the right end of the above vortex in Fig. 10. The axial length of this vortex is $87\Delta x_2$. There is again a strong correlation in the variations of $\frac{1}{2}|\omega|^2$, $\nabla^2 p$ and $-D$ (cf. Fig. 3(a)).

The cross-section of the core of this vortex is shown in Figs. 9(b) and (c) over the whole vortex and over $35 < s/\Delta x < 50$ (around the lowest D), respectively. The change of shape is substantial. The mean radius averaged over the whole vortices is $4.9 l_K$, and it is $5.8 l_K$ for vortices longer than the mean length. The mean value for longer vortices seems to approach around $6.1 l_K$. These values are greater by about 50% than those for the isotropic turbulence (§3.1).

The vortical regions defined by $D < 0$ occupy 14% of the total volume which is again too much to visualize their entire boundary. The 16% of the enstrophy is included in these vortical regions. The vortical regions defined by $\Delta > 0$ and $\nabla^2 p > 0$ occupy 70% and 44% volume, respectively.

Four vortices are picked up and shown in Fig. 10, where the color denotes the sum of the two largest eigenvalues of the pressure hessian. The green is the largest and the yellow is the lowest. The structure of individual vortices is now clearly visualized.

4 Concluding remarks

We have considered in this paper how to educe and visualize the swirling slender vortices from complicated turbulent motions. The sectional-swirl-and-pressure-minimum scheme is proposed as one of the objective eduction methods of low-pressure vortices. This scheme is composed of two steps; the trace of the vortex axes and the construction of the core. It is one of serious common problems that the amount of memory and computation load are too enormous to analyze the spatial structure and the temporal evolution of the three-dimensional vortical structures. Fortunately, we can relax this problem by the use of the above scheme in

the following two ways. First, by representing a vortex only by the central axes (the skeleton representation), we can save the data size drastically. Secondly, since the individual vortices can be marked and analyzed independently, it is possible to pick up only a few vortices to be investigated.

Finally, we would like to mention the coherent structures, among which may be counted the swirling slender vortex. Although the coherent or organized structures which keep their identity in turbulent flows over relatively long times and over wide space have attracted people's attention over these three decades, it does not seem to be unique but, on the contrary, rather arbitrary, to find and define some long-lived structures in continuous fluid motions. Many different kinds of coherent structures can be observed in principle depending upon which physical quantity we are focusing to (see [Hussain, 1986], [Robinson, 1991]). The way of understanding of turbulence may be influenced by the definition of coherent structure. Therefore, it is quite important to find and study such coherent structures that play dymanically essential roles.

Acknowledgements

The authors would like to thank Professor N.J. Zabusky for introducing us some relevant references on vortex visualization. Thanks also due to Dr. M. Tanaka for his kind offer of numerical data of homogeneous shear turbulence. This work was partially supported by a Grant-in-Aid for Scientific Research from the Ministry of Education, Science and Culture in Japan.

References

Banks, D. C., Singer, B. A., 1995, A predictor-corrector technique for visualizing unsteady flow. *IEEE Trans. on visualization and computer graphics*, **1**, 151-163.

Bernal, L.P., Roshko, A., 1986, Streamwise vortex structure in plane mixing layers. *J. Fluid Mech.*, **170**, 499-525.

Bernard, P. S., Thomas, J. M., Handler, R. A., 1993, Vortex dynamics and the productions of reynolds stress. *J. Fluid Mech.*, **253**, 385-419.

Brachet, M.E., Meneguzzi, M., Politano, H., Sulem, P.L., 1988, The dynamics of freely decaying two-dimensional turbulence. *J. Fluid Mech.*, **194**, 333-349.

Chong, M.S., Perry, A.E., Cantwell, B.J., 1990, A general classification of three-dimensional flow fields. *Phys. Fluids A*, **2**, 765-777.

Dallmann, U., 1983, Topological structures of three-dimensional flow separations. *DFVLR*, Rep. No. 221-82-A07, Göttingen. West Germany.

Douady, S., Couder, Y., Brachet, M.E., 1991, Direct observation of the intermittency of intense vorticity filaments in turbulence. *Phys. Rev. Lett.*, **67**, 983–986.

Hussain, F., 1986, Coherent structures and turbulence. *J. Fluid Mech.*, **173**, 303-356.

Iwayama, T., Okamoto, H., 1996, Reconsideration of a scaling theory in two-dimensional decaying turbulence. *Prog. Theor. Phys.*, **96**, 1061-71.

Jeong, J., Hussain, F., 1995, On the identification of a vortex. *J. Fluid Mech.*, **285**, 69-94.

Jeong, J., Hussain, F., Schoppa, W., Kim, J., 1997, Coherent structures near the wall in a turbulent channel flow. *J. Fluid Mech.*, **332**, 185-214.

Jiménez, J., Wray, A.A, Saffman, P.G., Rogallo, R.S., 1993, The structure of intense vorticity in isotropic turbulence. *J. Fluid Mech.*, **255**, 65-90.

Kida, S., Tanaka, M., 1992, Reynolds stress and vortical structure in a uniformly sheared turbulence. *J. Phys. Soc. Japan*, **61**, 4400-4417.

Kida, S., Tanaka, M., 1994, Dynamics of vortical structures in a homogeneous shear flow. *J. Fluid Mech.*, **274**, 43-68.

Kim, H.T., Kline, S.J., Reynolds, W.C., 1971, The production of turbulence near a smooth wall in a turbulent boundary layer. *J. Fluid Mech.*, **50**, 133-160.

Lesieur, M., Métais, O., 1996, New trends in large-eddy simulations of turbulence. *Annu. Rev. Fluid Mech.*, **28**, 45-82.

Lugt, H. J., 1979, The dilemma of defining a vortex. *Recent Developments in Theoretical and Experimental Fluid Mechanics,springer*, pages 309-321.

McWilliams, J.C., 1984, The emergence of isolated coherent vortices in turbulent flow. *J. Fluid Mech.*, **146**, 21-43.

Miura, H., Kida, S., 1997, Identification of tubular vortices in complex flows. *J. Phys. Soc. Japan* **66**, *1331-1334*.

Moin, P., Kim, J., 1982, Numerical investigation of turbulent channel flow. *J. Fluid Mech.*, **118**, 341-377.

Porter, D. H., Pouquet, A., Woodward, P. R., 1994, Kolmogorov-like spectra in decaying three-dimensional supersonic flows. *Phys. Fluids*, **6**, 2133-2142.

Robinson, S. K., 1991, Coherent motions in the turbulent boundary layer. *Ann. Rev. Fluid Mech.*, **23**, 601–39.

She, Z. S., Jackson, E., Orszag, S. A., 1991, Structures and dynamics of homogeneous turbulence: models and simulations. *Proc. R. Soc. Lond. A*, **434**, 101-124.

Siggia E. D., 1981, Numerical study of small scale intermittency in three dimensional turbulence. *J. Fluid Mech.*, **107**, 375-406.

Tanahashi, M., Miyauchi, T., Ikeda, J., 1997, Scaling law of coherent fine scale structure in homogeneous isotropic turbulence. *11th. Symp. on Turbulent Shear Flows* (to be published).

Tanaka, M., Kida, S., 1993, Characterization of vortex tubes and sheets. *Phys. Fluids A*, **5**, 2079-2082.

Villasenor J. and Vincent, A., 1992, An algorithm for space recognition and time tracking of vorticity tubes in turbulence. *COMP:Image Understanding*, **55**, 27-35.

Weiss, J., 1991, The dynamics of enstrophy transfer in two-dimensional hydrodynamics. *Physica D*, **48**, 273-294.

Wray, A.A., Hunt, J.C.R., 1990, Algorithms for classification of turbulent structures. *In Topological Fluid Mechanics* (ed. H.K. Moffatt & A. Tsinober) pp. 95—104. Cambridge University Press.

Yamamoto, K., Hosokawa, I., 1988 A decaying isotropic turbulence pursued by the spectral method. *J. Phys. Soc. Japan*, **57**, 1532-1535.

Figure captions

Figure 1. Isosurfaces of (a) the vorticity magnitude and (b) the Laplacian of pressure in isotropic turbulence. The thresholds are set so that each of them covers the 5% of the total volume.

Figure 2. The vortex skeletons in isotropic turbulence.

Figure 3. (a) The variations of D (solid line), $\frac{1}{2}|\omega|^2$ (thick broken line), p (dotted line) and $\nabla^2 p$ (thin broken line) along the axis of a vortex. Here, p is multiplied by 100. The cross-section of the core (b) in the whole vortex and (c) in range $25 < s/\Delta x < 35$.

Figure 4. The axial distributions of (a) The mean (solid line) and the standard deviation (broken line) of the core radius and (b) the circulation of a vortex.

Figure 5. The variations along a vortex of (a) the angles of the third eigenvector of the pressure hessian (solid line) and of the vorticity (broken line) from the skeleton, (b) the angles between the eigenvector of the pressure hessian and the vorticity, and (c) the angles of consecutive segments of the skeleton.

Figure 6. (a) The vortex skeletons (white lines) and 13 vortex cores (colored) in isotropic turbulence. (b) Close-up of (a). A part of core of the light-blue vortex is being gouged out by another vortex (green).

Figure 7. Isosurfaces of (a) the vorticity magnitude and (b) the Laplacian of pressure and (c) their union in homogeneous shear turbulence. The thresholds are set so that each of them covers the 5% of the total volume.

Figure 8. Vortex skeleton in homogeneous shear turbulence.

Figure 9. (a) The variations of D (solid line), $\frac{1}{2}|\omega|^2$ (thick broken line), p (dotted line) and $\nabla^2 p$ (thin broken line) along the axis of a vortex. Here, p is multiplied by 100. The cross-section of the core (b) in the whole vortex and (c) in range $35 < s/\Delta x < 50$.

Figure 10. The vortex skeletons (white lines) and 4 vortex cores (colored) in homogeneous shear turbulence.

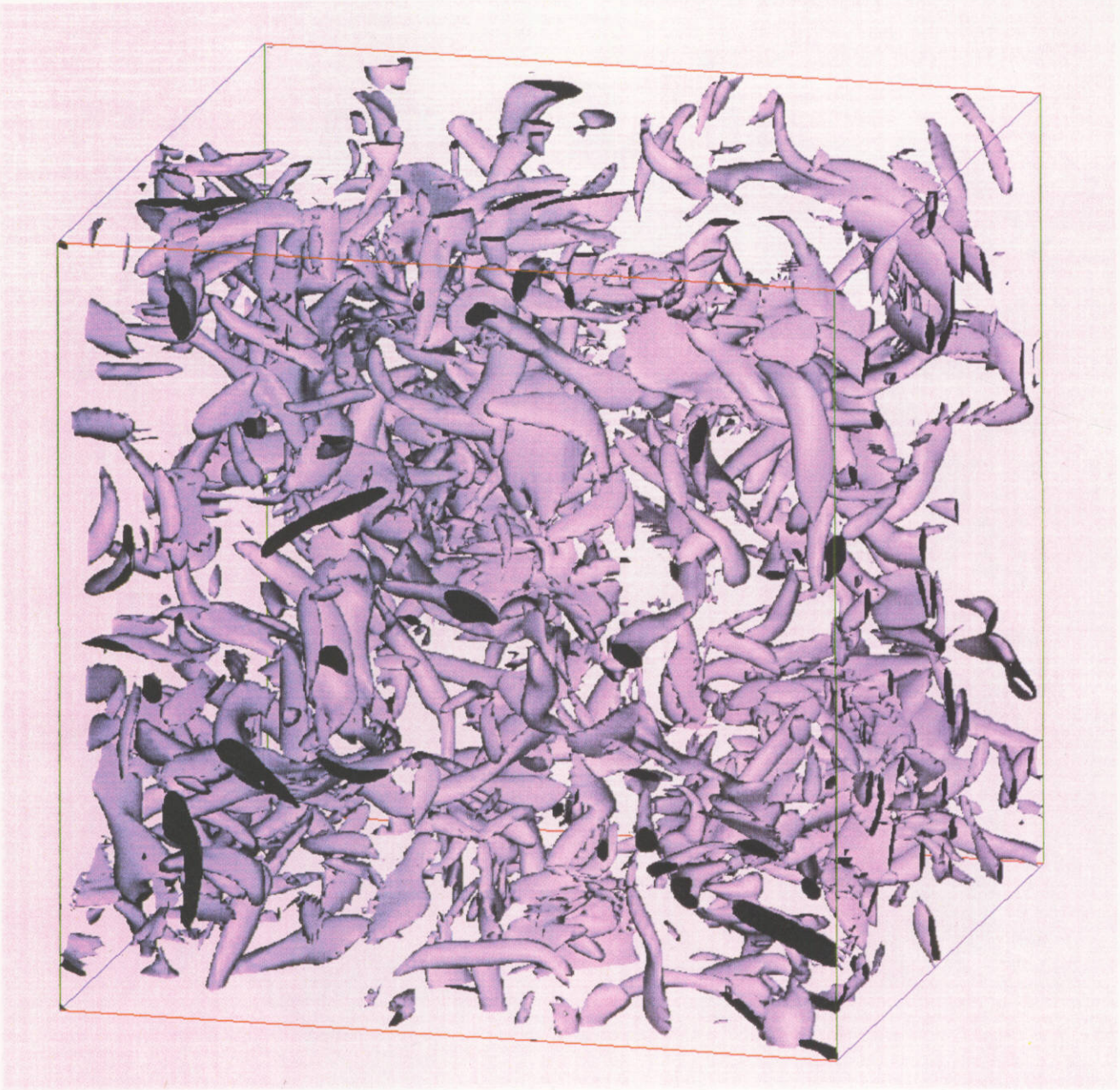

Figure 1: (a)

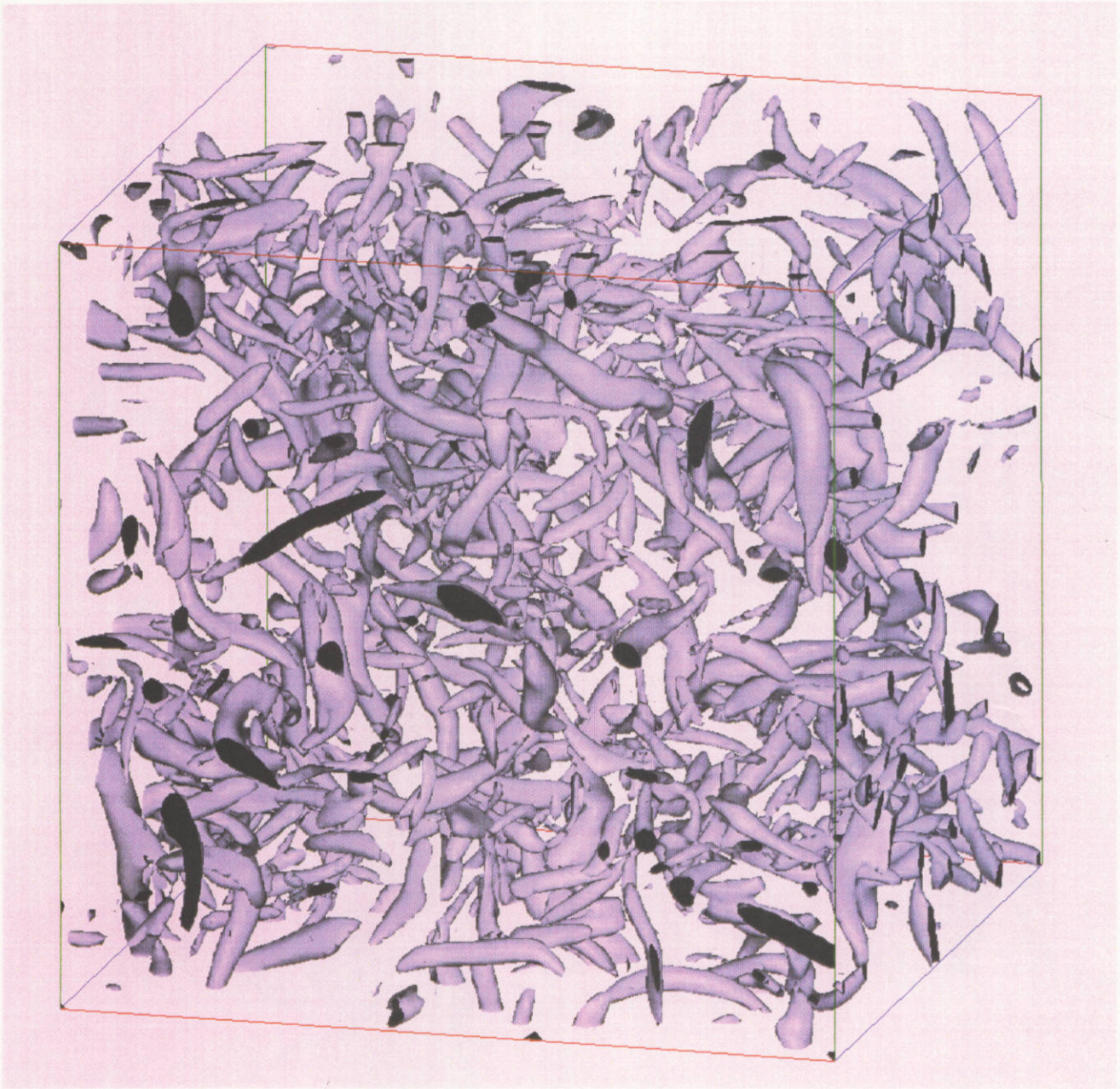

Figure 1: (b)

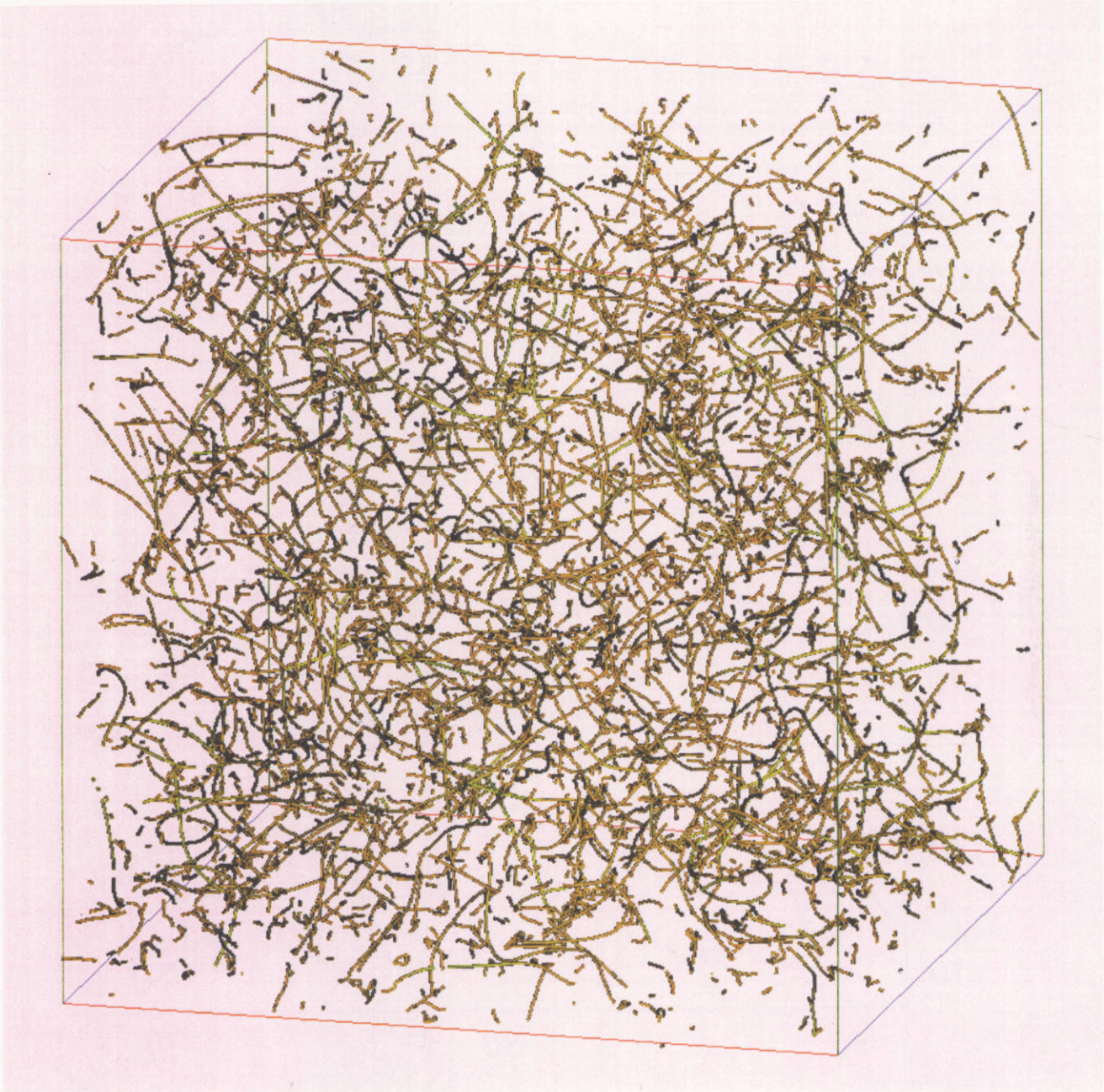

Figure 2:

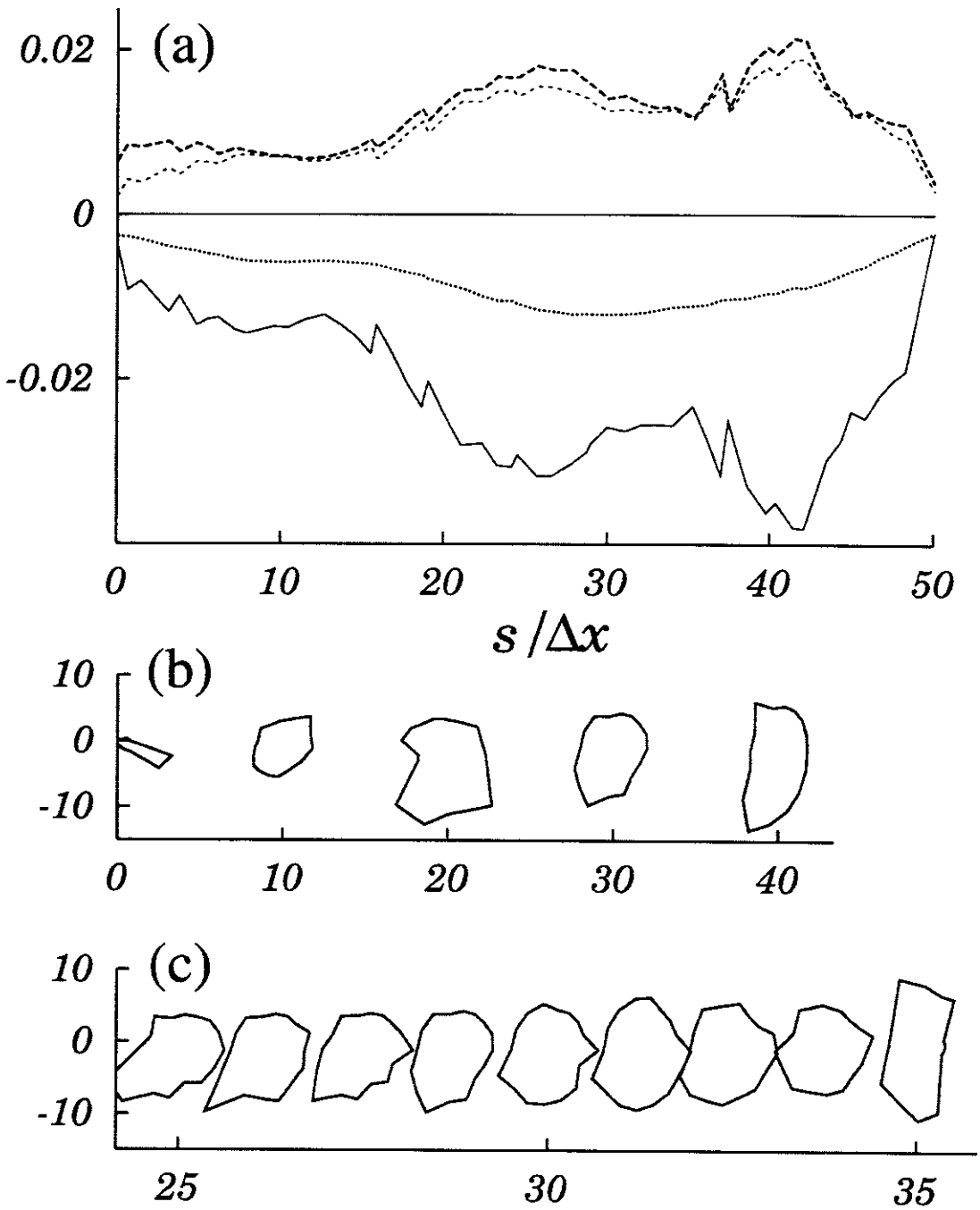

Figure 3:

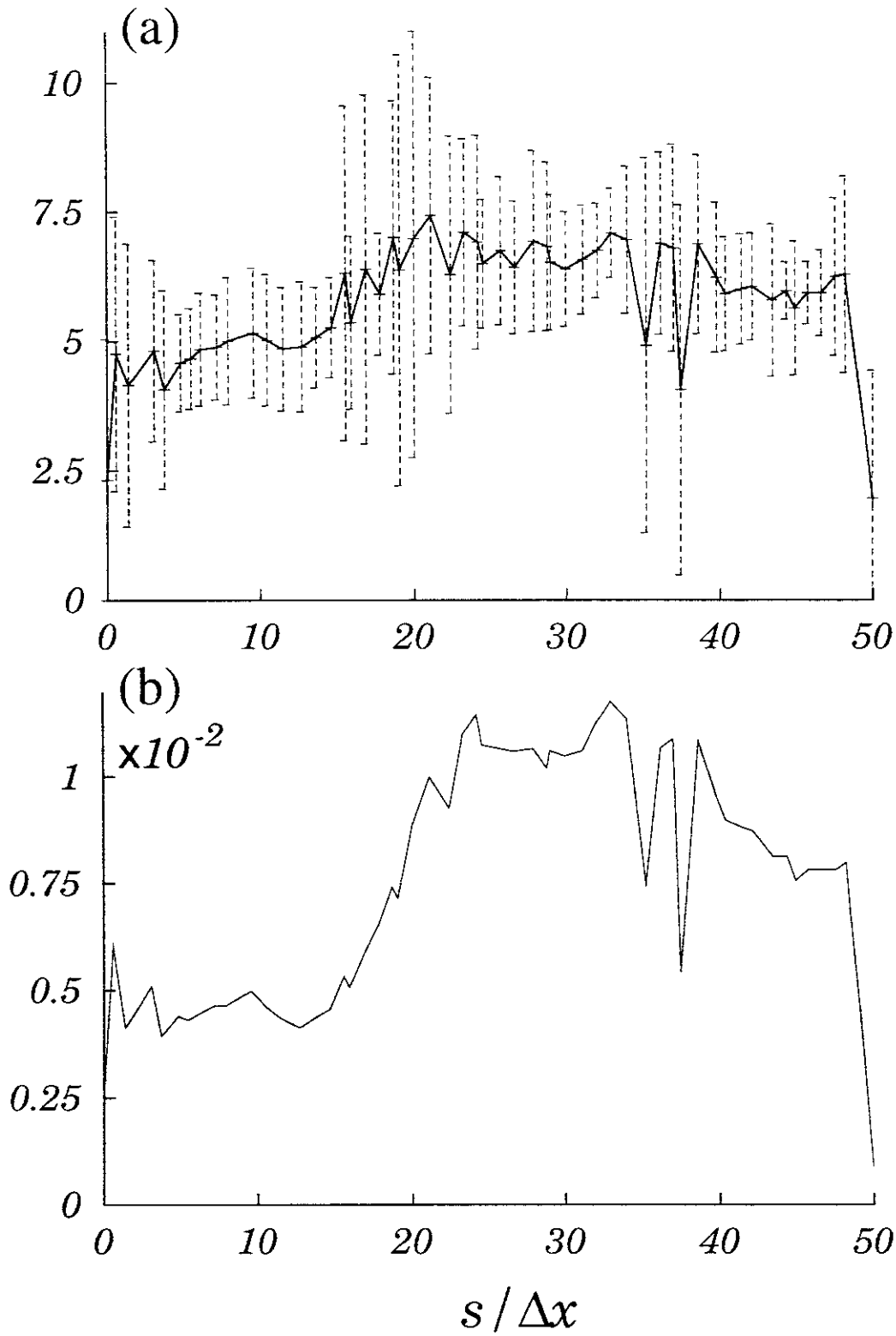

Figure 4:

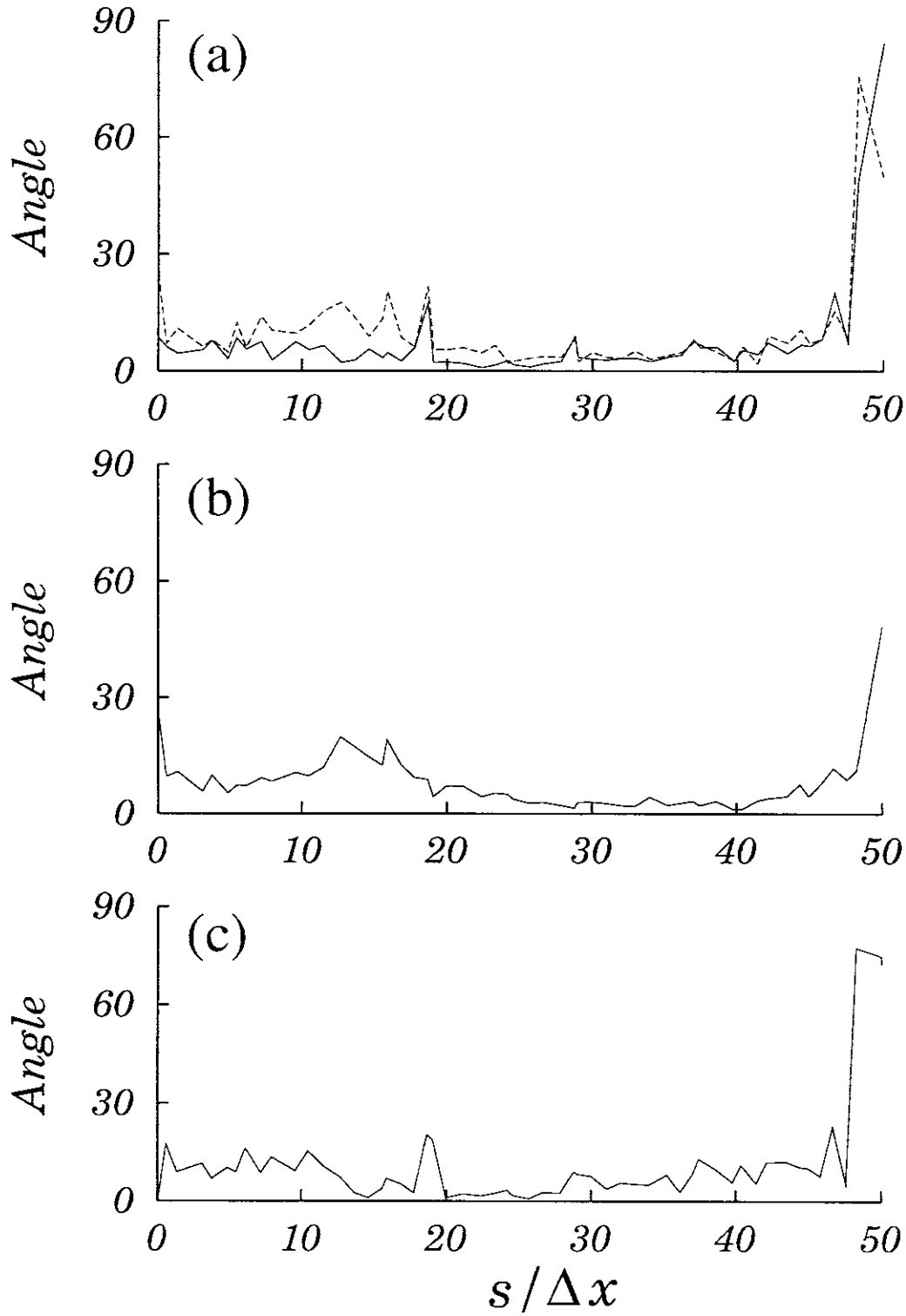

Figure 5:

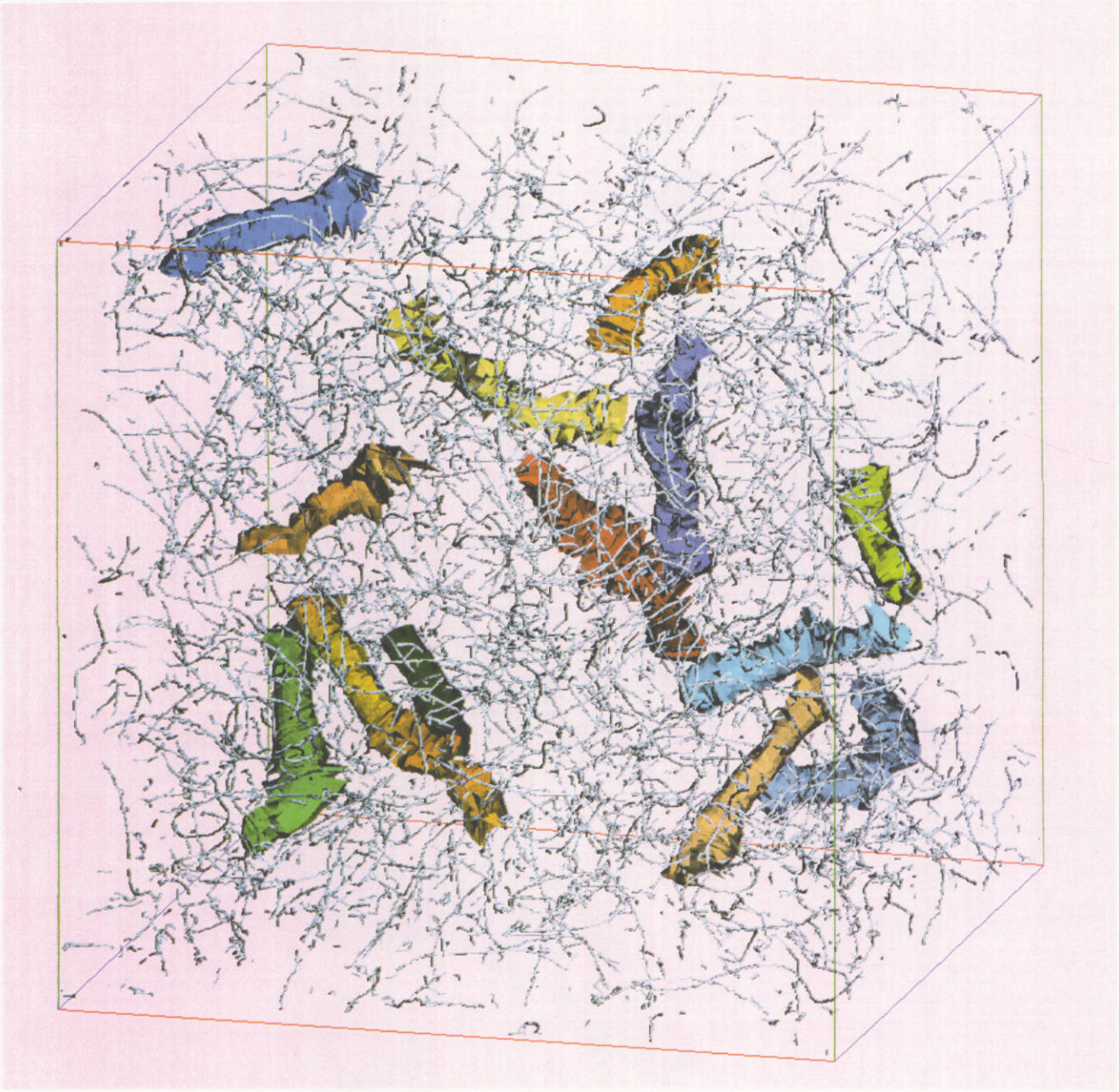

Figure 6: (a)

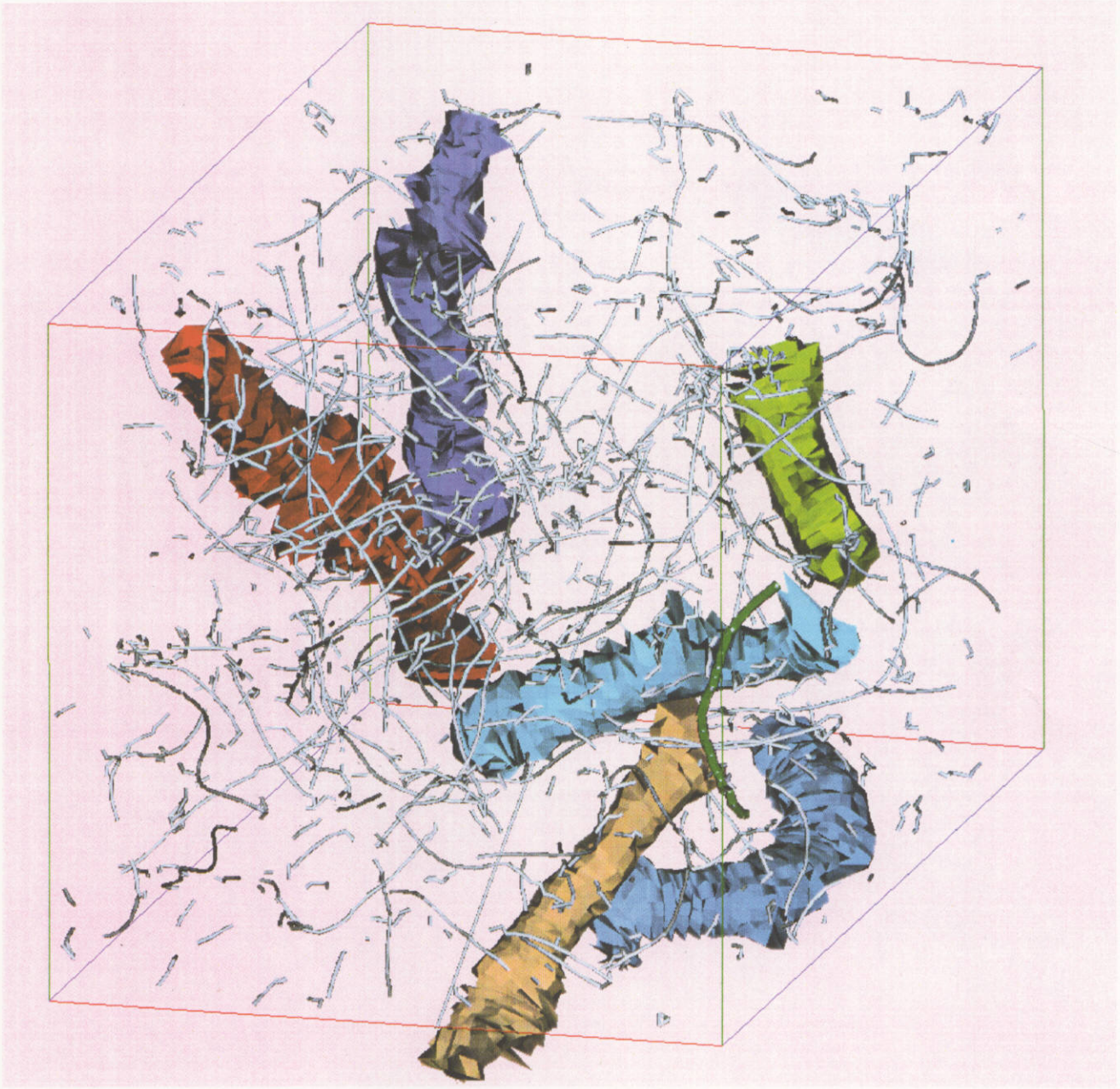

Figure 6: (b)

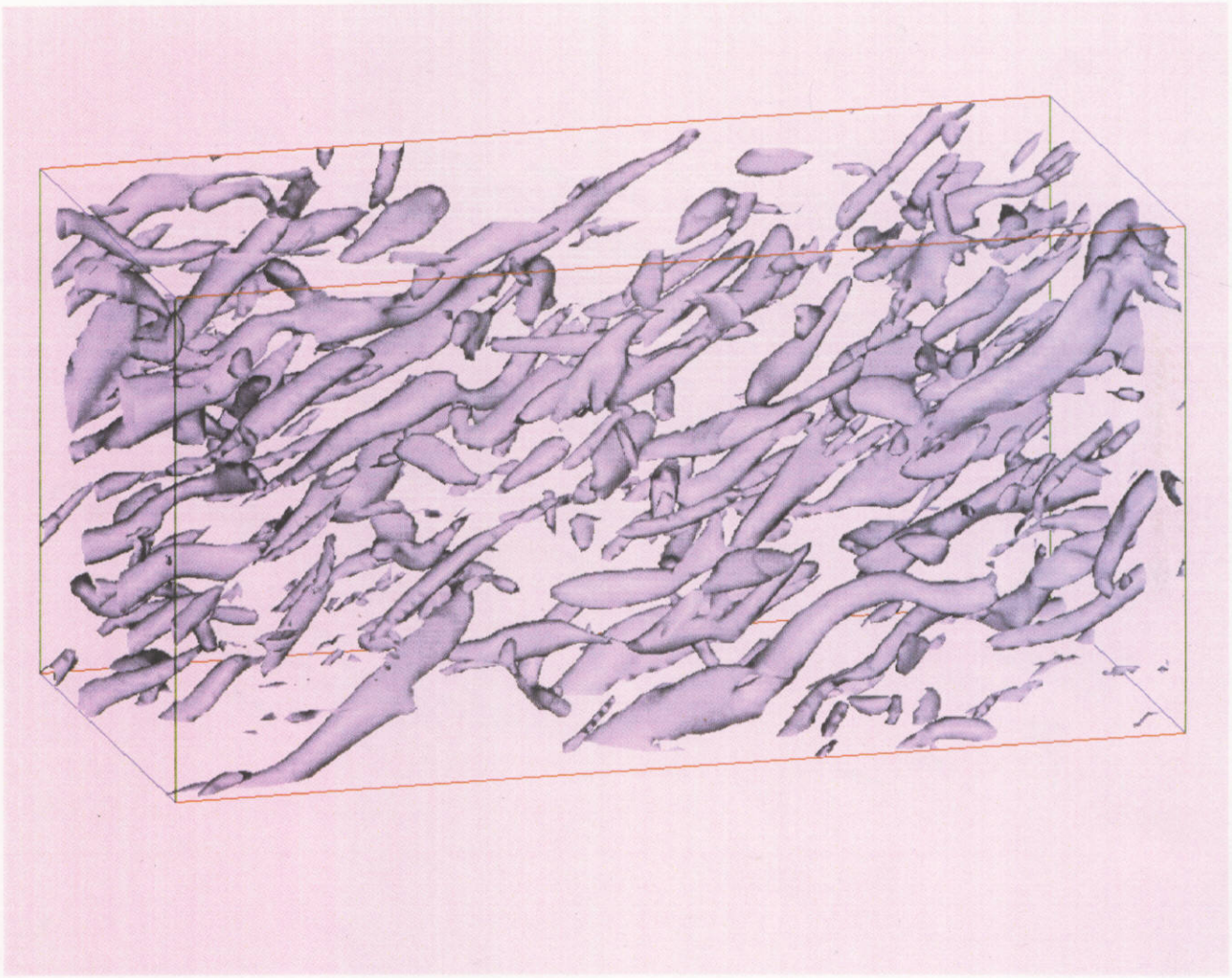

Figure 7: (a)

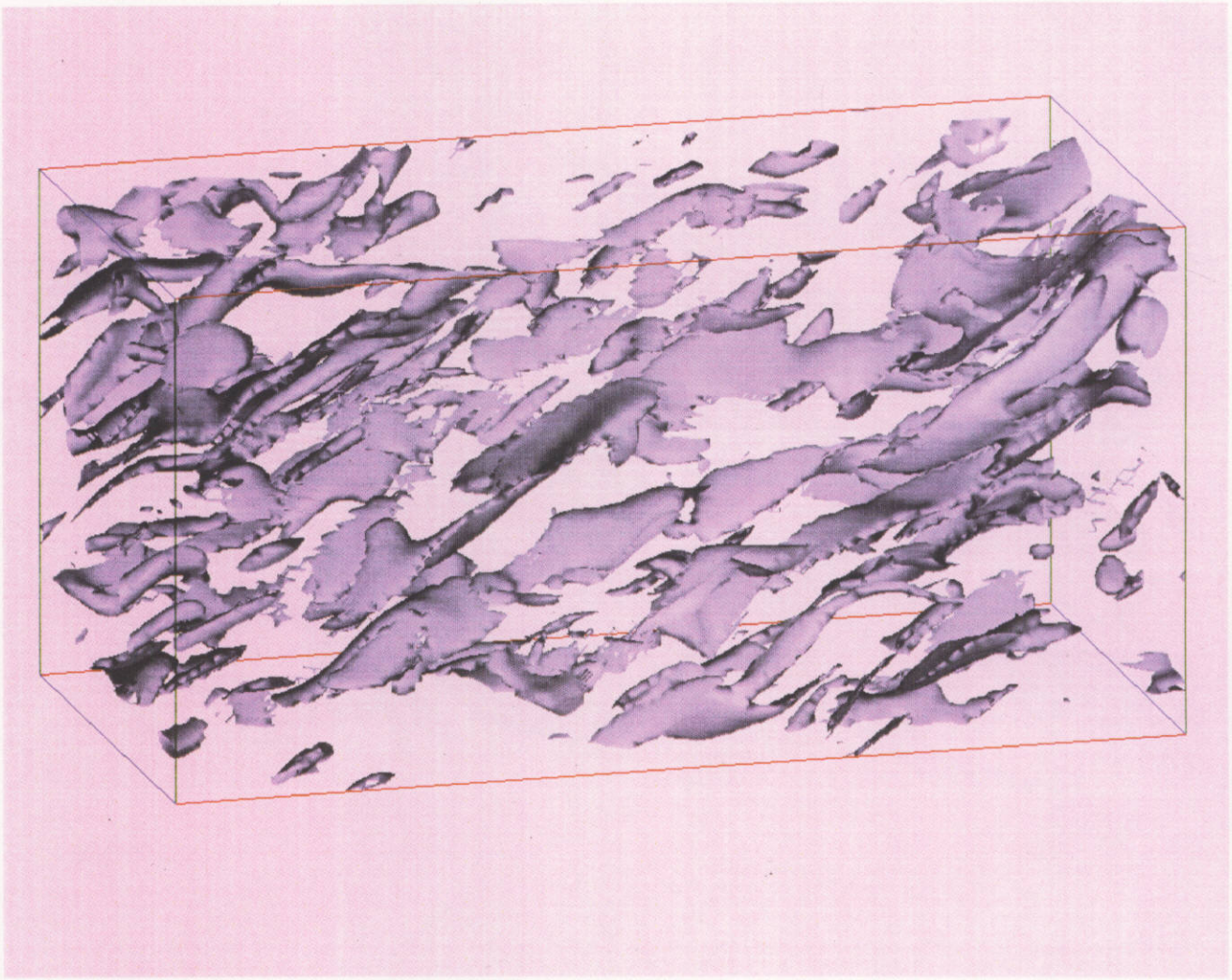

Figure 7: (b)

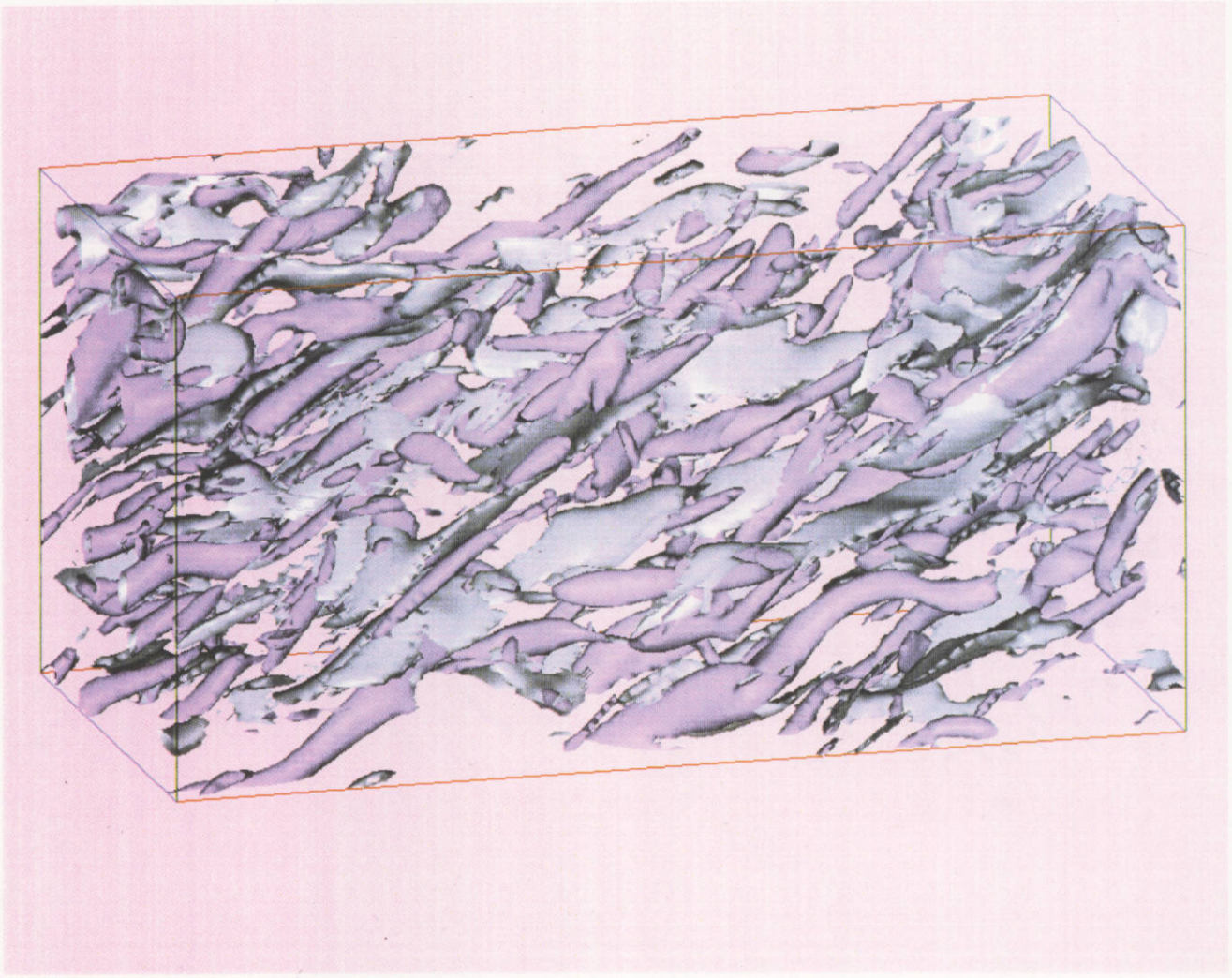

Figure 7: (c)

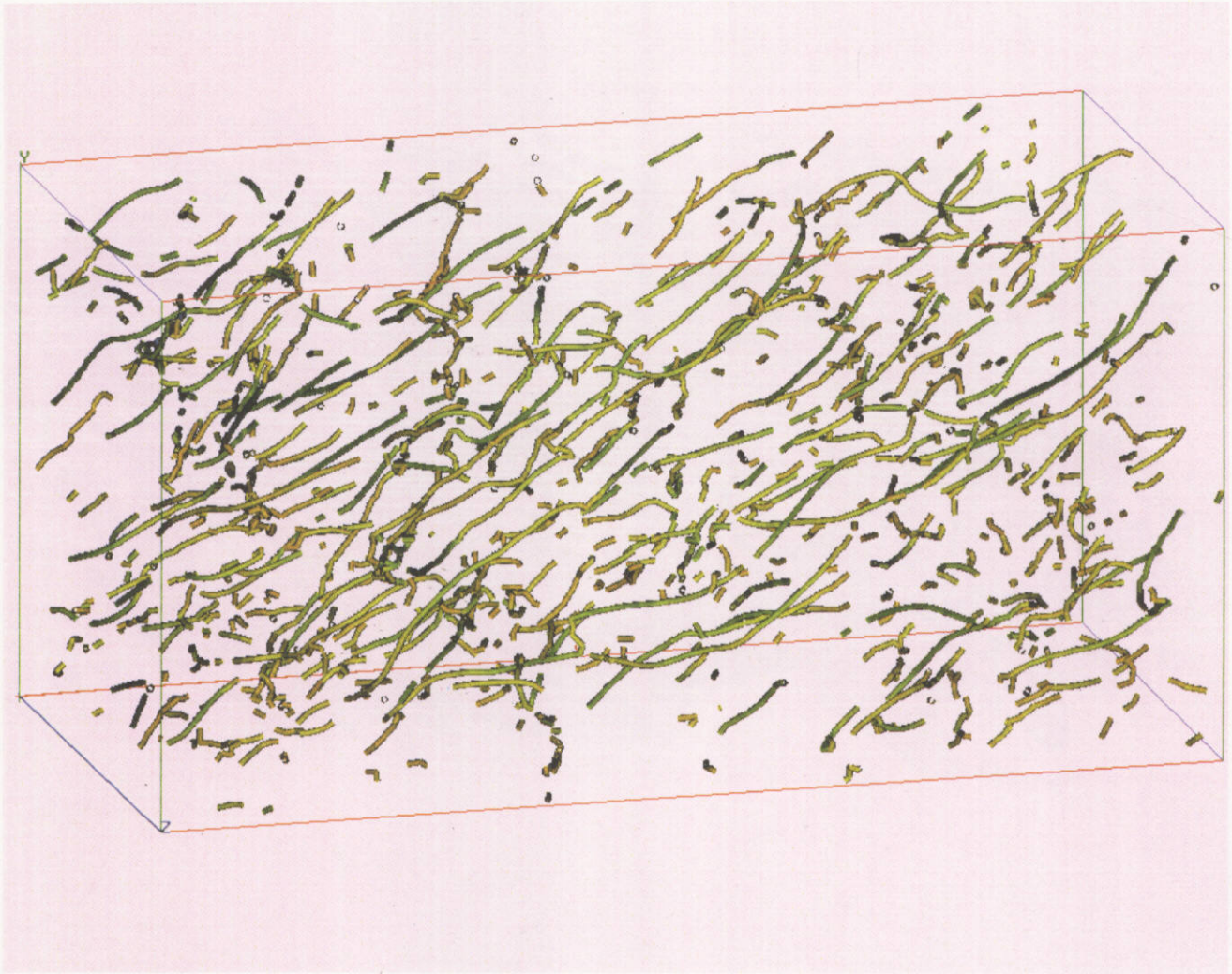

Figure 8:

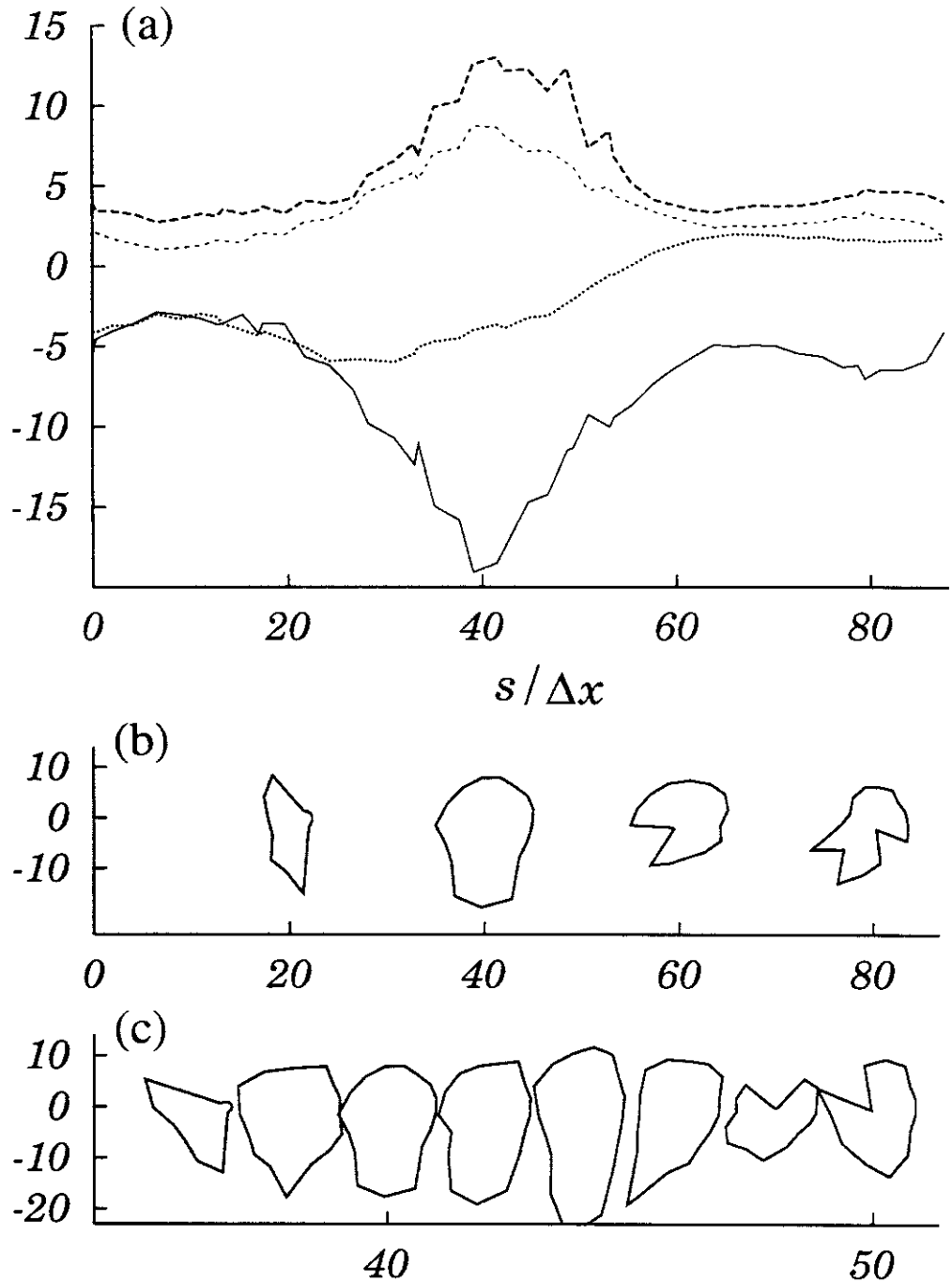
(a)
15
10
5
0
-5
-10
-15
0
20
40
60
80
s / Δx
(b)
10
0
-10
0
20
40
60
80
(c)
10
0
-10
-20
40
50

Figure 9:

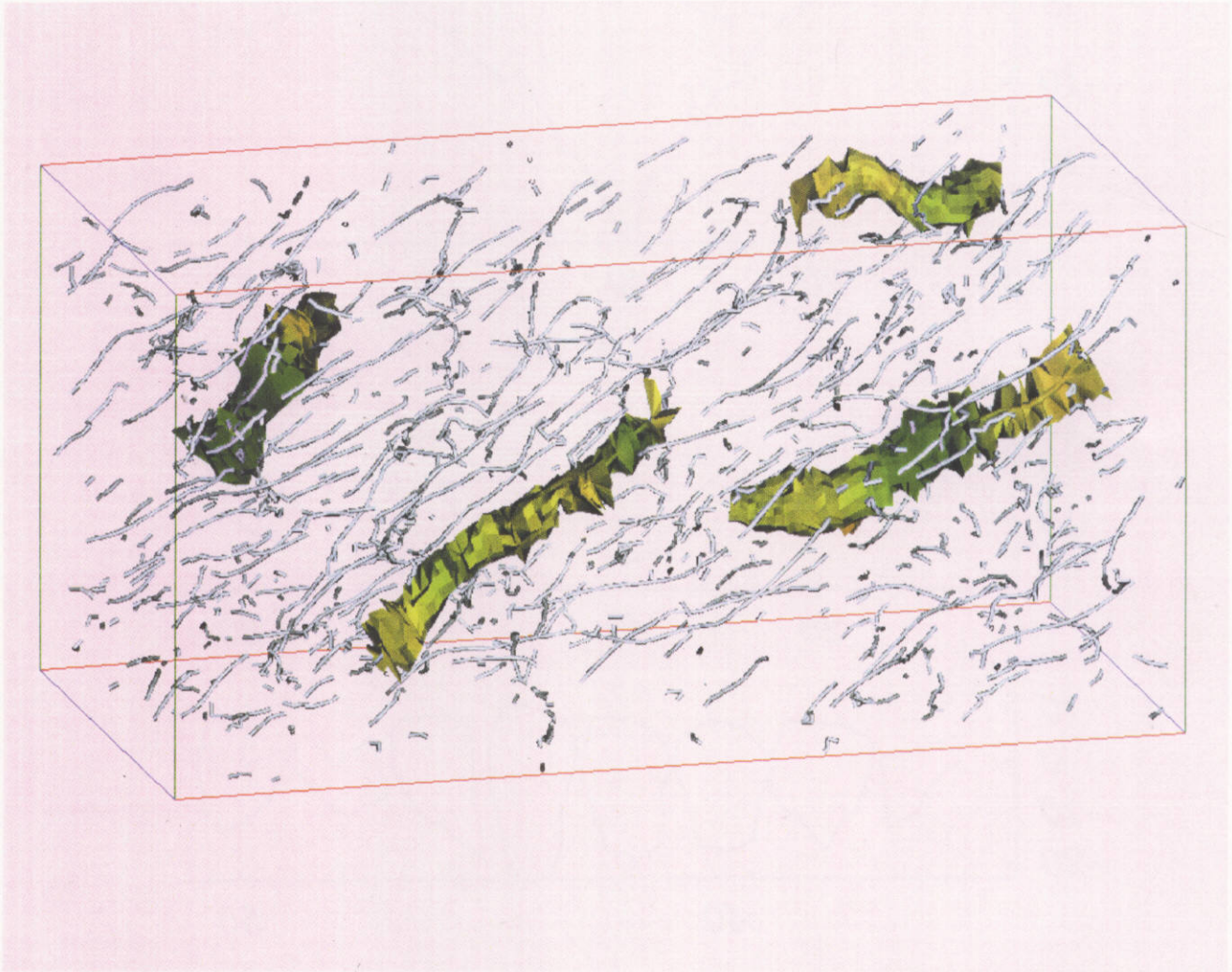

Figure 10:

Recent Issues of NIFS Series

NIFS-472 R. Kanno, N. Nakajima, H. Sugama, M. Okamoto and Y. Ogawa,
Effects of Finite-β and Radial Electric Fields on Neoclassical Transport in the Large Helical Device; Jan. 1997

NIFS-473 S. Murakami, N. Nakajima, U. Gasparino and M. Okamoto,
Simulation Study of Radial Electric Field in CHS and LHD; Jan. 1997

NIFS-474 K. Ohkubo, S. Kubo, H. Idei, M. Sato, T. Shimozuma and Y. Takita,
Coupling of Tilting Gaussian Beam with Hybrid Mode in the Corrugated Waveguide; Jan. 1997

NIFS-475 A. Fujisawa, H. Iguchi, S. Lee and Y. Hamada,
Consideration of Fluctuation in Secondary Beam Intensity of Heavy Ion Beam Prove Measurements; Jan. 1997

NIFS-476 Y. Takeiri, M. Osakabe, Y. Oka, K. Tsumori, O. Kaneko, T. Takanashi, E. Asano, T. Kawamoto, R. Akiyama and T. Kuroda,
Long-pulse Operation of a Cesium-Seeded High-Current Large Negative Ion Source; Jan. 1997

NIFS-477 H. Kuramoto, K. Toi, N. Haraki, K. Sato, J. Xu, A. Ejiri, K. Narihara, T. Seki, S. Ohdachi, K. Adati, R. Akiyama, Y. Hamada, S. Hirokura, K. Kawahata and M. Kojima,
Study of Toroidal Current Penetration during Current Ramp in JIPP T-IIU with Fast Response Zeeman Polarimeter; Jan., 1997

NIFS-478 H. Sugama and W. Horton,
Neoclassical Electron and Ion Transport in Toroidally Rotating Plasmas; Jan. 1997

NIFS-479 V.L. Vdovin and I.V. Kamenskij,
3D Electromagnetic Theory of ICRF Multi Port Multi Loop Antenna; Jan. 1997

NIFS-480 W.X. Wang, M. Okamoto, N. Nakajima, S Murakami and N. Ohyabu,
Cooling Effect of Secondary Electrons in the High Temperature Divertor Operation; Feb. 1997

NIFS-481 K. Itoh, S.-I. Itoh, H. Soltwisch and H.R. Koslowski,
Generation of Toroidal Current Sheet at Sawtooth Crash; Feb. 1997

NIFS-482 K. Ichiguchi,
Collisionality Dependence of Mercier Stability in LHD Equilibria with Bootstrap Currents; Feb. 1997

NIFS-483 S. Fujiwara and T. Sato,
Molecular Dynamics Simulations of Structural Formation of a Single

Polymer Chain: Bond-orientational Order and Conformational Defects; Feb. 1997

NIFS-484 T. Ohkawa,
Reduction of Turbulence by Sheared Toroidal Flow on a Flux Surface; Feb. 1997

NIFS-485 K. Narihara, K. Toi, Y. Hamada, K. Yamauchi, K. Adachi, I. Yamada, K. N. Sato, K. Kawahata, A. Nishizawa, S. Ohdachi, K. Sato, T. Seki, T. Watari, J. Xu, A. Ejiri, S. Hirokura, K. Ida, Y. Kawasumi, M. Kojima, H. Sakakita, T. Ido, K. Kitachi, J. Koog and H. Kuramoto,
Observation of Dusts by Laser Scattering Method in theJIPPT-IIU Tokamak Mar. 1997

NIFS-486 S. Bazdenkov, T. Sato and The Complexity Simulation Group,
Topological Transformations in Isolated Straight Magnetic Flux Tube; Mar. 1997

NIFS-487 M. Okamoto,
Configuration Studies of LHD Plasmas; Mar. 1997

NIFS-488 A. Fujisawa, H. Iguchi, H. Sanuki, K. Itoh, S. Lee, Y. Hamada, S. Kubo, H. Idei, R. Akiyama, K. Tanaka, T. Minami, K. Ida, S. Nishimura, S. Morita, M. Kojima, S. Hidekuma, S.-I. Itoh, C. Takahashi, N. Inoue, H. Suzuki, S. Okamura and K. Matsuoka,
Dynamic Behavior of Potential in the Plasma Core of the CHS Heliotron/Torsatron; Apr. 1997

NIFS-489 T. Ohkawa,
Pfirsch - Schlüter Diffusion with Anisotropic and Nonuniform Superthermal Ion Pressure; Apr. 1997

NIFS-490 S. Ishiguro and The Complexity Simulation Group,
Formation of Wave-front Pattern Accompanied by Current-driven Electrostatic Ion-cyclotron Instabilities; Apr. 1997

NIFS-491 A. Ejiri, K. Shinohara and K. Kawahata,
An Algorithm to Remove Fringe Jumps and its Application to Microwave Reflectometry; Apr. 1997

NIFS-492 K. Ichiguchi, N. Nakajima, M. Okamoto,
Bootstrap Current in the Large Helical Device with Unbalanced Helical Coil Currents; Apr. 1997

NIFS-493 S. Ishiguro, T. Sato, H. Takamaru and The Complexity Simulation Group,
V-shaped dc Potential Structure Caused by Current-driven Electrostatic Ion-cyclotron Instability; May 1997

NIFS-494 K. Nishimura, R. Horiuchi, T. Sato,
Tilt Stabilization by Energetic Ions Crossing Magnetic Separatrix in Field-Reversed Configuration; June 1997

NIFS-495 T. -H. Watanabe and T. Sato,
Magnetohydrodynamic Approach to the Feedback Instability; July 1997

NIFS-496 K. Itoh, T. Ohkawa, S. -I.Itoh, M. Yagi and A. Fukuyama
Suppression of Plasma Turbulence by Asymmetric Superthermal Ions; July 1997

NIFS-497 T. Takahashi, Y. Tomita, H. Momota and Nikita V. Shabrov,
Collisionless Pitch Angle Scattering of Plasma Ions at the Edge Region of an FRC; July 1997

NIFS-498 M. Tanaka, A.Yu Grosberg, V.S. Pande and T. Tanaka,
Molecular Dynamics and Structure Organization in Strongly-Coupled Chain of Charged Particles; July 1997

NIFS-499 S. Goto and S. Kida,
Direct-interaction Approximation and Reynolds-number Reversed Expansion for a Dynamical System; July 1997

NIFS-500 K. Tsuzuki, N. Inoue, A. Sagara, N. Noda, O. Motojima, T. Mochizuki, T. Hino and T. Yamashina,
Dynamic Behavior of Hydrogen Atoms with a Boronized Wall; July 1997

NIFS-501 I. Viniar and S. Sudo,
Multibarrel Repetitive Injector with a Porous Pellet Formation Unit; July 1997

NIFS-502 V. Vdovin, T. Watari and A. Fukuyama,
An Option of ICRF Ion Heating Scenario in Large Helical Device; July 1997

NIFS-503 E. Segre and S. Kida,
Late States of Incompressible 2D Decaying Vorticity Fields; Aug. 1997

NIFS-504 S. Fujiwara and T. Sato,
Molecular Dynamics Simulation of Structural Formation of Short Polymer Chains; Aug. 1997

NIFS-505 S. Bazdenkov and T. Sato
Low-Dimensional Model of Resistive Interchange Convection in Magnetized Plasmas; Sep. 1997

NIFS-506 H. Kitauchi and S. Kida,
Intensification of Magnetic Field by Concentrate-and-Stretch of Magnetic Flux Lines; Sep. 1997

NIFS-507 R.L. Dewar,
Reduced form of MHD Lagrangian for Ballooning Modes; Sep. 1997

NIFS-508 Y.-N. Nejoh,
Dynamics of the Dust Charging on Electrostatic Waves in a Dusty Plasma with Trapped Electrons; Sep.1997

NIFS-509 E. Matsunaga, T.Yabe and M. Tajima,
Baroclinic Vortex Generation by a Comet Shoemaker-Levy 9 Impact; Sep. 1997

NIFS-510 C.C. Hegna and N. Nakajima,
On the Stability of Mercier and Ballooning Modes in Stellarator Configurations; Oct. 1997

NIFS-511 K. Orito and T. Hatori,
Rotation and Oscillation of Nonlinear Dipole Vortex in the Drift-Unstable Plasma; Oct. 1997

NIFS-512 J. Uramoto,
Clear Detection of Negative Pionlike Particles from H_2 Gas Discharge in Magnetic Field; Oct. 1997

NIFS-513 T. Shimozuma, M. Sato, Y. Takita, S. Ito, S. Kubo, H. Idei, K. Ohkubo, T. Watari, T.S. Chu, K. Felch, P. Cahalan and C.M. Loring, Jr,
The First Preliminary Experiments on an 84 GHz Gyrotron with a Single-Stage Depressed Collector; Oct. 1997

NIFS-514 T. Shjmozuma, S. Morimoto, M. Sato, Y. Takita, S. Ito, S. Kubo, H. Idei, K. Ohkubo and T. Watari,
A Forced Gas-Cooled Single-Disk Window Using Silicon Nitride Composite for High Power CW Millimeter Waves; Oct. 1997

NIFS-515 K. Akaishi,
On the Solution of the Outgassing Equation for the Pump-down of an Unbaked Vacuum System; Oct. 1997

NIFS-516 *Papers Presented at the 6th H-mode Workshop (Seeon, Germany)*; Oct. 1997

NIFS-517 John L. Johnson,
The Quest for Fusion Energy; Oct. 1997

NIFS-518 J. Chen, N. Nakajima and M. Okamoto,
Shift-and-Inverse Lanczos Algorithm for Ideal MHD Stability Analysis; Nov. 1997

NIFS-519 M. Yokoyama, N. Nakajima and M. Okamoto,
Nonlinear Incompressible Poloidal Viscosity in L=2 Heliotron and Quasi-Symmetric Stellarators; Nov. 1997

NIFS-520 S. Kida and H. Miura,
Identificaiton and Analysis of Vortical Structures; Nov. 1997